Comment on "Direct photodetachment of F^- by mid-infrared few-cycle femtosecond laser pulses"

G. F. Gribakin* and S. M. K. Law†
Center for Theoretical Atomic, Molecular and Optical Physics, Queen's University Belfast, Belfast BT7 1NN, United Kingdom
(Received 18 July 2016; published 15 November 2016; corrected 20 December 2016)

Multiphoton detachment of F^- by strong few-cycle laser pulses was studied by Shearer and Monteith using a Keldysh-type approach [Phys. Rev. A **88**, 033415 (2013)]. We believe that this work contained errors in the calculation of the detachment amplitude and photoelectron spectra. We describe the necessary corrections to the theory and show that the results, in particular, the interference features of the photoelectron spectra, appear noticeably different. Corrected results are also in better agreement with the detachment probabilities determined by the R-matrix with time dependence method [Hassouneh *et al.*, Phys. Rev. A **91**, 031404(R) (2015)].

DOI: 10.1103/PhysRevA.94.057401

In Ref. [1] direct photodetachment of F^- by a strong linearly polarized laser field was considered using the Keldysh-type approach (KTA) [2] generalized to few-cycle pulses [3]. Such methods are useful in general for studying strong-field effects in few-cycle pulses; see, e.g., Ref. [4]. The study was performed for an N-cycle pulse with the vector potential of the form

$$\mathbf{A}(t) = A_0\hat{\mathbf{z}}\,\sin^2\left(\frac{\omega t}{2N}\right)\sin(\omega t+\alpha), \tag{1}$$

where A_0 is the peak amplitude, ω is the carrier frequency, and α is the carrier-envelope phase (CEP). Photoelectron momentum, angular, and energy distributions were generated for a $N=4$ cycle laser pulse with a range of peak intensities and mid-infrared wavelengths, while examining effects related to above-threshold channel closures and variation of the CEP.

A calculation similar to that of Ref. [1] was also used to identify the effect of electron rescattering in short-pulse multiphoton detachment from F^- computed using the R matrix with time dependence (RMT) method [5]. Subsequently, an error in the KTA calculations was uncovered [6]. It concerned the phase factors of the contributions to the detachment amplitude that arose from successive saddle points in the KTA calculation for a p-wave electron. Upon correction, the KTA results showed a better agreement with the RMT photoelectron spectra [5,6]. We believe that the same error affected the results of Ref. [1]. In this Comment we show that the interference features of the photoelectron momentum and angular distributions and the energy spectra are distinctly different from those of Ref. [1] when calculated correctly. We use atomic units throughout, unless stated otherwise.

Using the Keldysh-like approach [2] for the N-cycle pulse (1), one finds the detachment amplitude for an initial state with orbital and magnetic quantum numbers l and m as [see Eq. (16) of Ref. [1]]

$$A_{\mathbf{p}} = -(2\pi)^{3/2}A\sum_{\mu=1}^{2(N+1)}(\pm)^l Y_{lm}(\hat{\mathbf{p}}_\mu)\frac{\exp[if(t_\mu)]}{\sqrt{-if''(t_\mu)}}, \tag{2}$$

where $\mathbf{p}$ is the final photoelectron momentum and A is the asymptotic normalization constant of the bound electron wave function (for F^- we use $A=0.7$ [7]). Equation (2) involves a sum over $2(N+1)$ saddle points t_μ in the complex time plane, $\mathbf{p}_\mu$ and $f(t_\mu)$ being the classical electron momentum and action, respectively, evaluated at the saddle points. The terms in the sum in Eq. (2) contain a phase factor $(\pm)^l \equiv (\pm 1)^l$ that alternates (for an odd l) between the contributions from successive saddle points. When the spherical function $Y_{lm}(\hat{\mathbf{p}}_\mu)\equiv Y_{lm}(\Theta,\varphi)$ in Eq. (2) is evaluated for complex vectors $\mathbf{p}_\mu$, the polar angle Θ is determined by

$$\cos\Theta = \sqrt{1+p_\perp^2/\kappa_j^2}, \quad \sin\Theta = \mp i p_\perp/\kappa_j, \tag{3}$$

where $p_\perp$ is the component $\mathbf{p}$ perpendicular to the z axis, and $\kappa_j = \sqrt{2|E_j|}$ parametrizes the energy E_j of the bound state for each fine-structure component $j=3/2,1/2$ of F^- ($l=1$). The sign in $\sin\Theta$ alternates in the opposite way to $(\pm)$ in Eq. (2) and gives rise to an additional m-dependent phase factor. The final expression for the differential detachment probability of an electron from the state l,m reads

$$\frac{dw_{lm}^{(j)}}{d^3\mathbf{p}} = \frac{A^2}{4\pi}(2l+1)\frac{(l-|m|)!}{(l+|m|)!}\left|P_l^{|m|}\left(\sqrt{1+p_\perp^2/\kappa_j^2}\right)\right|^2 \times\left|\sum_{\mu=1}^{2(N+1)}(\pm)^{l+m}\frac{\exp[if(t_\mu)]}{\sqrt{-if''(t_\mu)}}\right|^2, \tag{4}$$

where $P_l^{|m|}$ is the associated Legendre function. The superscript j is introduced into expression (4) to indicate the detachment from the spin-orbit sublevel j of the ion, which contributes with the statistical factor $(2j+1)/(2l+1)$ to the total detachment probability. The numerical values of κ_j for each fine-structure state of F^- are $\kappa_{3/2}=0.4998$ and $\kappa_{1/2}=0.5035$ (using the electron affinity of F^- from Ref. [8]). Note that Eq. (4) takes a similar form to Eq. (33) from Ref. [2] in the case of the long periodic pulse.

The photoelectron momentum densities are axially symmetric and can be obtained from Eq. (4) by taking $\mathbf{p}$ in the Cartesian momentum plane (p_x,p_z),

$$\sum_j\frac{2j+1}{2l+1}\sum_{m=-l}^{l}\frac{dw_{lm}^{(j)}}{d^3\mathbf{p}}. \tag{5}$$

*g.gribakin@qub.ac.uk
†slaw08@qub.ac.uk

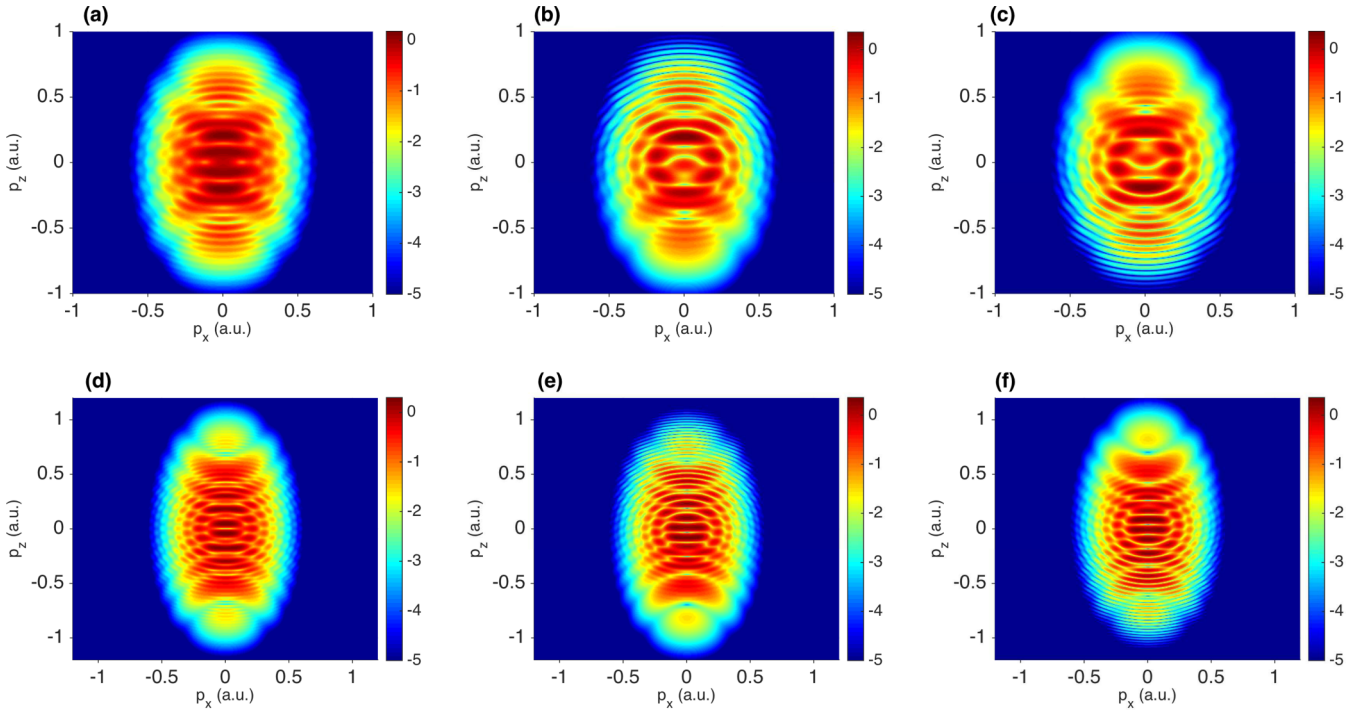

FIG. 1. Logarithmic momentum densities for photodetachment of F^- by a four-cycle laser pulse with peak intensity of 1.3×10^{13} W/cm^2. The top and bottom rows correspond to $\lambda = 1300$ and 1800 nm, respectively, calculated for $\alpha = 0$ [(a) and (d)], $\alpha = \pi/2$ [(b) and (e)], and $\alpha = 3\pi/2$ [(c) and (f)], (a) $\lambda = 1300\,\text{nm}\,\alpha = 0$, (b) $\lambda = 1300\,\text{nm}\,\alpha = \pi/2$, (c) $\lambda = 1300\,\text{nm}\,\alpha = 3\pi/2$, (d) $\lambda = 1800\,\text{nm}\,\alpha = 0$, (e) $\lambda = 1800\,\text{nm}\,\alpha = \pi/2$, (f) $\lambda = 1800\,\text{nm}\,\alpha = 3\pi/2$.

The photoelectron angular distribution is obtained by integrating Eq. (4) over the electron energy $E_e = p^2/2$,

$$\frac{dw}{d\theta} = 2\pi \sin\theta \sum_j \sum_{m=-l}^{l} \frac{2j+1}{2l+1} \int_0^\infty \frac{dw_{lm}^{(j)}}{d^3\mathbf{p}} \sqrt{2E_e} dE_e, \quad (6)$$

where θ is the polar angle. The photoelectron energy spectrum is given by

$$\frac{dw}{dE_e} = 2\pi\sqrt{2E_e} \sum_j \sum_{m=-l}^{l} \frac{2j+1}{2l+1} \int_0^\pi \frac{dw_{lm}^{(j)}}{d^3\mathbf{p}} \sin\theta\, d\theta, \quad (7)$$

and the total detachment probability is

$$w = \int_0^\infty \frac{dw}{dE_e} dE_e \equiv \int_0^\pi \frac{dw}{d\theta} d\theta. \quad (8)$$

In Ref. [5] and, we believe, in Ref. [1] too, the presence of the phase factor $(\pm)^{l+m}$ in the sum over the saddle points in Eq. (4) was overlooked in the calculations. As a result, the detachment probability for p electrons ($l = 1$) was computed correctly for $m = \pm 1$, but incorrectly for $m = 0$, with the interference contributions between the odd and even saddle points added with the wrong sign. Since $m = 0$ electron states give a dominant contribution to the detachment signal, this error affected the interference patterns of the photoelectron momentum and energy distributions presented in Ref. [1] (see [5] and erratum [6]). In addition, we have found that the magnitudes of the photoelectron angular and energy spectra in Figs. 4–7 of Ref. [1] are incorrect. This is in part due to the extra spin factor 2 in Eq. (19) of Ref. [1], which was erroneously retained when accounting for the fine-structure splitting in Eq. (23) of Ref. [1], and also affected the KTA results in Ref. [5]. The purpose of this Comment is to present correct photoelectron distributions for the same wavelengths and other laser-pulse parameters as used originally in Ref. [1].

Figure 1 displays logarithmic photoelectron momentum densities for photodetachment of F^- by a four-cycle pulse with peak intensity of 1.3×10^{13} W/cm^2 and carrier wavelength of 1300 and 1800 nm, for CEP values $\alpha = 0, \pi/2$, and $3\pi/2$. Compared with Fig. 2 of Ref. [1], the correct interference patterns appear more diffuse, lacking any sharp features. Figures 1(a) and 1(d) show closer agreement with the momentum densities predicted by the RMT method [5]. At the same time, the overall forward-backward asymmetry along the p_z direction (for $\alpha = \pi/2$ and $3\pi/2$) is generally unaffected, since this characteristic depends on the symmetry of the laser field only.

Figure 2 shows photoelectron angular distributions for F^- for a four-cycle pulse with CEP $\alpha = 0$, wavelengths 1300 and 1800 nm, and intensities of 7.7×10^{12}, 1.1×10^{13}, and 1.3×10^{13} W/cm^2. Because of the errors mentioned earlier, these angular distributions are very different, both in shape and magnitude, from the (incorrect) results in Fig. 5 of Ref. [1]. The oscillatory structure of the distributions is related to the minimum number of photons that needs to be absorbed near the peak of the pulse, $n_{\min}$ [determined by the integer part of $(U_\mathbf{p} + |E_j|)/\omega + 1$ for a given ponderomotive energy $U_\mathbf{p} = A_0^2/4$]. Analysis of Fig. 2 shows that the angular distributions are characterized by a local maximum (minimum) in the direction perpendicular to the field ($\theta = \pi/2$) when $n_{\min}$ is odd (even). This can be seen in Figs. 2(a), 2(d), and 2(f) corresponding to $n_{\min} = 5, 9$, and 11, respectively, and in contrast to the original

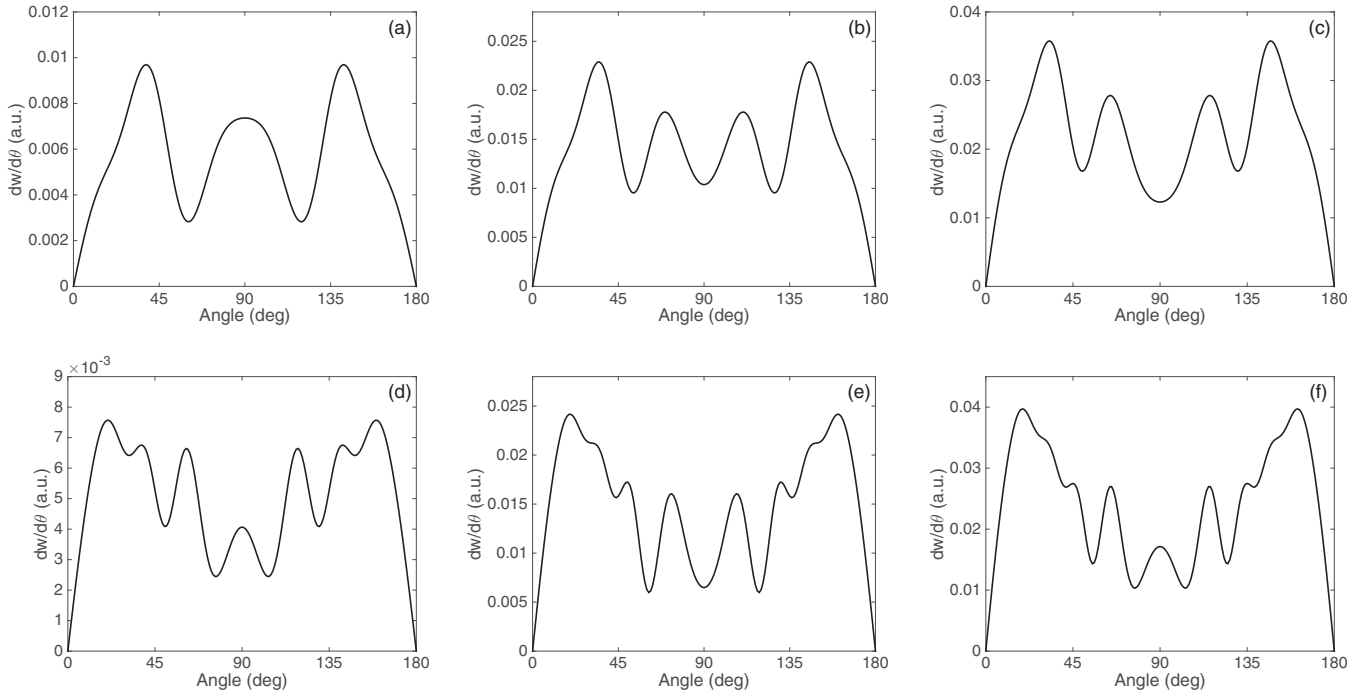

FIG. 2. Photoelectron angular distributions for F^- for a four-cycle pulse with $\lambda = 1300$ (top row) and 1800 nm (bottom row), CEP $\alpha = 0$, and peak intensities 7.7×10^{12}, 1.1×10^{13}, and 1.3×10^{13} W/cm^2 (left, central, and right columns, respectively); (a)–(c) correspond to $n_{\min} = 5$, 6, and 6, and (d)–(f) to $n_{\min} = 9$, 10, and 11-photon detachment, respectively.

(incorrect) results of [1] where a central minimum for odd $n_{\min}$ was noted. The effect of channel closure with increasing intensity gives rise to even $n_{\min} = 6$, 6, and 10 and a minimum at $\theta = \pi/2$, as seen in Figs. 2(b), 2(c), and 2(e), respectively. This behavior is in agreement with the observation that for a long periodic pulse the n-photon detachment rate is exactly zero at $\theta = \pi/2$ for odd $n + l + m$ [2], and the fact that $m = 0$ dominates the photoelectron spectrum. Figure 2 also indicates that electron emission at angles close to the direction of the field (i.e., within $0 \leqslant \theta \leqslant 45^\circ$ and $135^\circ \leqslant \theta \leqslant 180^\circ$) is much stronger here in comparison to Ref. [1], and in better accord with the momentum maps in Fig. 1.

Figure 3 displays the angular distributions computed for CEP values $\alpha = \pi/2$ and $3\pi/2$, and corrects Fig. 6 or Ref. [1].

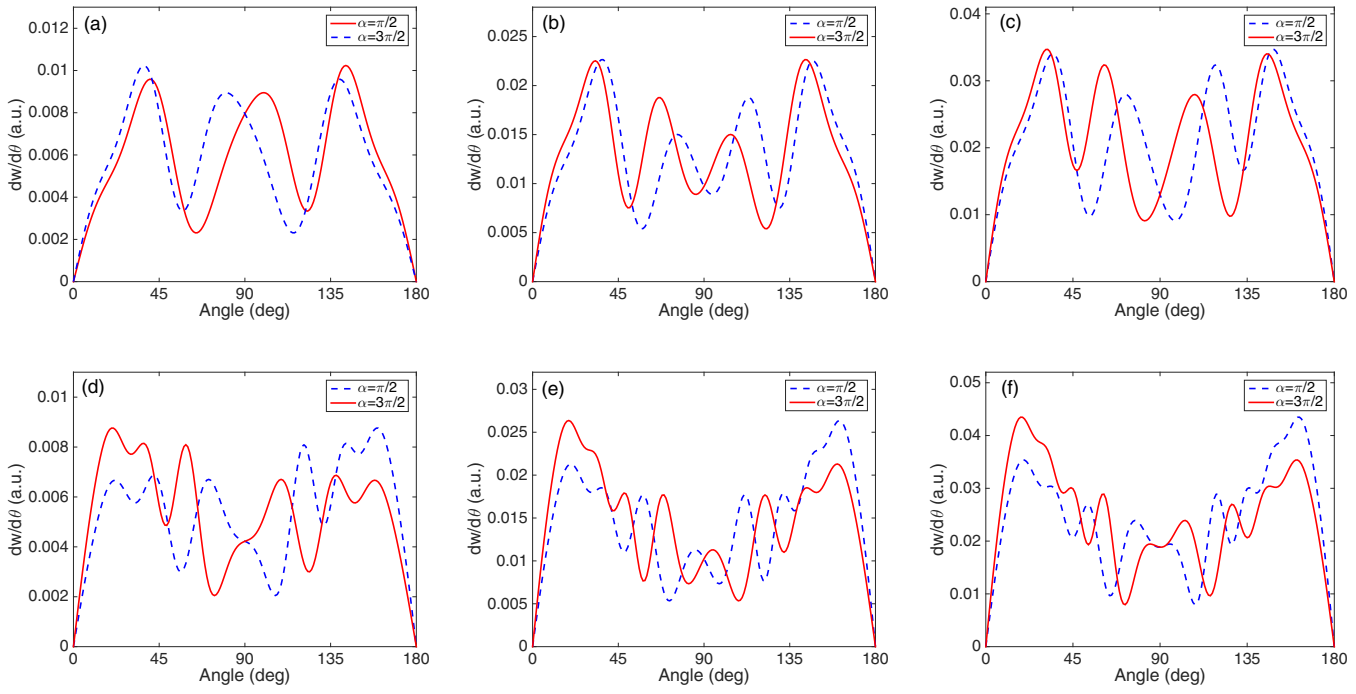

FIG. 3. Angular distributions as in Fig. 2 but for $\alpha = \pi/2$ (dashed) and $3\pi/2$ (solid).

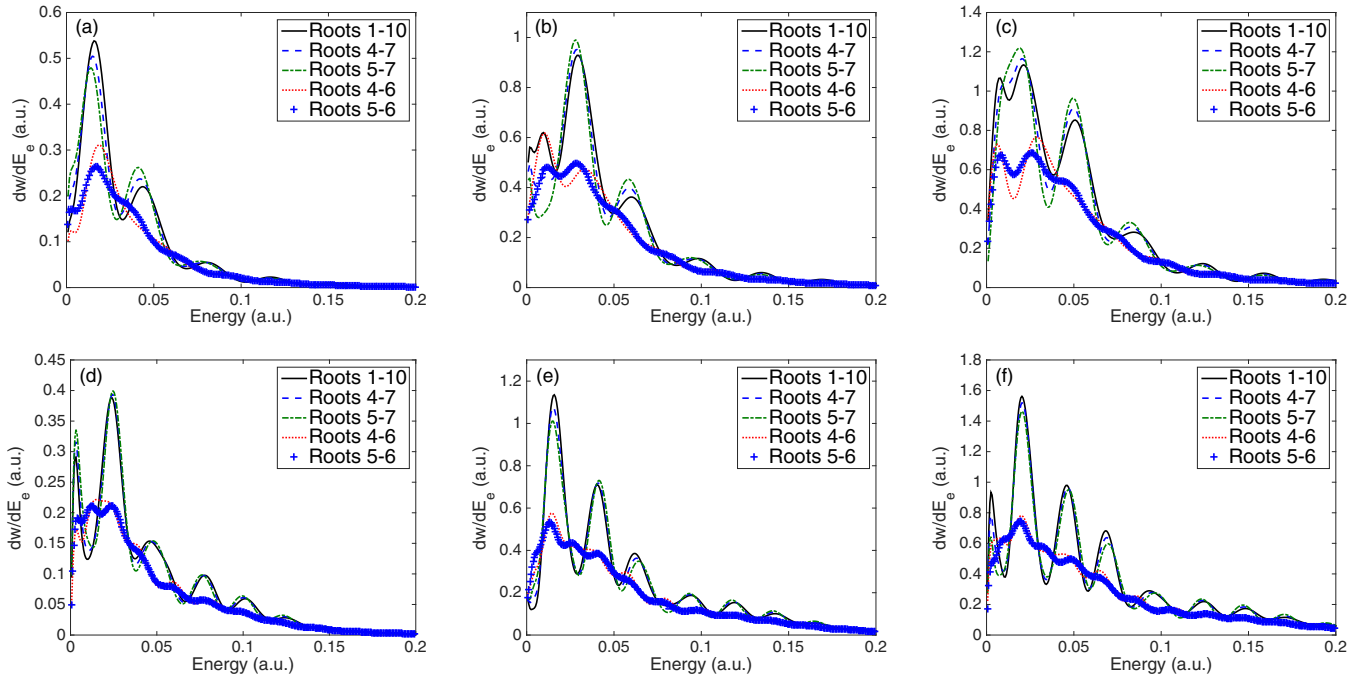

FIG. 4. Photoelectron energy spectra of F^- (in atomic units) calculated according to Eq. (7) for a four-cycle laser pulse with $\lambda = 1300$ (top row) and 1800 nm (bottom row), CEP $\alpha = 0$, and peak intensities 7.7×10^{12}, 1.1×10^{13}, and 1.3×10^{13} W/cm^2 (left, central, and right columns, respectively). Partial contributions from selected saddle points ("roots") are also shown.

While the shapes are very different, the degree of asymmetry on the angular distributions for these CEP values is consistent with that seen in Ref. [1].

Figure 4 presents the photoelectron energy spectra for a four-cycle pulse with $\alpha = 0$ and the same wavelengths and intensities as in Fig. 2. It also shows the spectra obtained by including only two, three, or four saddle points closest to the center of the pulse. Comparing with Fig. 7 of Ref. [1], we see that the shapes and magnitudes of the correct spectra are quite different from those reported in Ref. [1]. We note that the spectra shown in Figs. 4(c) and 4(f) (corresponding to intensity 1.3×10^{13} W/cm^2 and wavelength 1300 and 1800 nm, respectively) show better agreement with those calculated using RMT [5] in the low-energy region. This can be seen from the comparison of the corrected KTA spectra in Figs. 2(c) and 2(d) of Ref. [6] with the original (incorrect) KTA spectra in Fig. 3 of Ref. [5]. The present KTA detachment probabilities are also in much better agreement with the values obtained using the R matrix with time dependence method (RMT) [5] (see below).

For completeness, Table I gives the total detachment probability for F^- for all wavelengths and intensities considered. The total probability w [Eq. (8)] calculated for CEP values $\alpha = 0$ and $\pi/2$ is displayed in columns 4 and 5, respectively ($\alpha = 3\pi/2$ and $\pi/2$ give equivalent results). As shown above, correct phases of the terms in the amplitude are crucial for the shapes of the photoelectron momentum, angular, and energy distributions. However, they play a relatively small role in the total detachment probability. We have checked that if the latter is calculated by omitting the $(\pm)^{l+m}$ factor in Eq. (4), the total detachment probability is within 1%–2% of the values given in Table I. In fact, the total detachment probability obtained by neglecting the interference terms [i.e., by adding the modulus-squared values of the individual saddle-point

TABLE I. Total detachment probabilities w for photodetachment of F^- for a four-cycle pulse at wavelengths 1300 and 1800 nm, and different peak intensities I and CEP phases $\alpha = 0$ and $\pi/2$.

λ	I	$n_{\min}$	Present calculation				RMT[a]	
(nm)	(W/cm^2)		$w(\alpha = 0)$	$w(\alpha = \pi/2)$	$w_{\text{no-int}}$[b]	w_{lp}[c]	1	2
1300	7.7×10^{12}	5	0.0178	0.0185	0.0174	0.0181	0.018	0.011
	1.1×10^{13}	6	0.0443	0.0412	0.0448	0.0416	0.045	0.031
	1.3×10^{13}	6	0.0687	0.0659	0.0683	0.0753	0.065	0.044
1800	7.7×10^{12}	9	0.0159	0.0170	0.0165	0.0165	0.020	0.013
	1.1×10^{13}	10	0.0468	0.0461	0.0475	0.0497	0.055	0.034
	1.3×10^{13}	11	0.0752	0.0768	0.0754	0.0789	0.080	0.052

[a]Total detachment probabilities from RMT calculations [5], models 1 and 2.
[b]Obtained by adding modulus-squared contributions from each saddle point in Eq. (4).
[c]Detachment probability per period for a long pulse, $w_{\text{lp}} = (2\pi/\omega)dw/dt$ (see text for details).

contributions in Eq. (4)], $w_{\text{no-int}}$, is within few percent of the correct value. This shows that the interference of the photoelectron wave packets produced at different laser-field maxima does not lead to much suppression or enhancement of electron emission, but only to some spatial redistribution of the photoelectron flux. The values of $w_{\text{no-int}}$ shown in column 6 of Table I are also practically independent of the CEP (with differences $\sim 0.01\%$).

Shown in the seventh column of Table I are the detachment probabilities *per period* w_{lp} determined from the KTA detachment rates in a long periodic pulse, dw/dt [2]. They are close to the detachment probabilities in the four-cycle pulse, which implies that, effectively, the detachment in the four-cycle pulse is dominated by the central, strongest-field cycle. A similar agreement was seen in Ref. [3] (Table II) which compared detachment probabilities of H^- in a five-cycle pulse with the corresponding one-period long-pulse probabilities from Ref. [2]. Also shown in the last two columns of Table I are the detachment probabilities obtained in the RMT calculations [5] using two descriptions of the F atom: a single-configuration approximation (model 1), and a five-configuration expansion (model 2). For $\lambda = 1300$ nm the KTA results are very close to those of RMT model 1, while for $\lambda = 1800$ nm the KTA detachment probabilities fall between those of models 1 and 2. This is a much better agreement than in the original paper [5], which reported incorrect KTA numbers [6].

Additionally, it is interesting to note that the total detachment probabilities in the short pulse are slightly greater for $\alpha = \pi/2$ than for $\alpha = 0$ if n_{min} is odd, but slightly smaller when n_{min} is even. This effect is entirely due to interference. It can be explained by the fact that for $\alpha = \pi/2$ the time-dependent electric field $\mathbf{E}(t) = -d\mathbf{A}/dt$ acquires its maximum peak magnitude twice within two central half-cycles, whereas for $\alpha = 0$ the field reaches its peak value once at the middle of the pulse. By comparing the angular distributions (Figs. 2 and 3) for odd and even n_{min} we see that, for $\alpha = \pi/2$, constructive interference is more prominent for odd n_{min} near the $\theta = \pi/2$ direction relative to the field, while for even n_{min}, destructive interference is more pronounced for angles near $\theta = \pi/2$. This gives slightly higher (lower) total detachment probabilities seen in Table I for $\alpha = \pi/2$ when n_{min} is odd (even).

In conclusion, the photoelectron spectra presented in Ref. [1] were incorrect, in part due to the omission of the m-dependent phase factor in the sum over the saddle points that gives the amplitude. Using the correct phase factor is crucial for obtaining correct interference features of the photoelectron momentum and angular distributions.

We thank H. W. van der Hart and A. C. Brown for useful discussions. S.M.K.L. acknowledges funding from DEL-NI under the programme for government.

[1] S. F. C. Shearer and M. R. Monteith, Phys. Rev. A **88**, 033415 (2013).
[2] G. F. Gribakin and M. Yu. Kuchiev, Phys. Rev. A **55**, 3760 (1997).
[3] S. F. C. Shearer, M. C. Smyth, and G. F. Gribakin, Phys. Rev. A **84**, 033409 (2011).
[4] D. B. Milosevic, G. G. Paulus, D. Bauer, and W. Becker, J. Phys. B **39**, R203 (2006).
[5] O. Hassouneh, S. Law, S. F. C. Shearer, A. C. Brown, and H. W. van der Hart, Phys. Rev. A **91**, 031404(R) (2015).
[6] O. Hassouneh, S. M. K. Law, S. F. C. Shearer, A. C. Brown, and H. W. van der Hart, Phys. Rev. A **93**, 069901(E) (2016).
[7] E. E. Nikitin and B. M. Smirnov, *Atomic and Molecular Processes* (Nauka, Moscow, 1988).
[8] T. Andersen, H. K. Haugen, and H. Hotop, J. Phys. Chem. Ref. Data **28**, 1511 (1999).